

# OPTIMAL FORMATION DEPLOYMENT USING RELATIVE CONSTRAINTS

Michael Volle\*

## Abstract

In the near future, it is likely that missions will employ distributed systems of spacecraft that operate in the vicinity of libration point orbits (LPOs). These systems could take the form of a constellation or a formation, such as an interferometric array. The use of multiple spacecraft imposes additional navigation requirements on the mission, most notably in the form of relative positioning requirements. These relative positioning requirements are often more stringent than the requirements placed on the formation's location in absolute space. In fact, the initial deployment of the formation can be optimized with respect to relative targeting conditions for the final state. This paper examines a method of optimizing the deployment of a formation of spacecraft about a reference halo orbit using relative dynamics and relative targeting conditions. The equations of motion relative to the reference halo orbit are derived and calculated in a rotating frame. The relative targeting conditions are used to specify an arbitrary formation size and shape, and zero relative velocity. Indirect methods of optimization are used to form a time-constrained, finite-burn, minimum fuel problem. A thrust-coast-thrust control law is enforced, and solutions are examined with regard to the distribution of propellant cost.

## INTRODUCTION

The use of distributed spacecraft systems creates several unique challenges for mission planning and design. A few of these challenges that must be addressed are: the even distribution of propellant cost across the formation, the mitigation of collision between spacecraft, the relative navigation and control of the formation, the absolute navigation and control of the formation, and the maneuver planning or optimization of formation deployment/reconfiguration maneuvers. Given the applications of spacecraft formations (for uses such as interferometry), the relative positioning requirements for a formation are often more stringent and therefore more important than the absolute positioning requirements. Therefore, when it comes to optimizing formation maneuvers, it may be advantageous to consider the relative positioning requirements instead of targeting points that are fixed with respect to a reference frame.

Additionally, there is a strong likelihood that spacecraft formations will be deployed to low-acceleration environments such as LPO's. In this highly non-linear environment, many of the simplifying assumptions used in relative dynamics are not accurate enough. Methods like assuming a circular orbit or using a first-order approximation do not provide the accuracy required when dealing with the relative positioning requirements of a formation. Therefore, it is also advantageous to compose the problem of formation deployment in a framework of fully non-linear relative dynamics.

Other works have considered the problem of optimizing the deployment or reconfiguration of a formation of spacecraft. These works have covered a range of dynamical models and orbit types. Yang, et al.<sup>1</sup> used Hill's equations to create a hybrid optimization algorithm that uses both calculus of variations and a genetic algorithm (GA) to optimize the reconfiguration of a formation. However,

---

\*Aerospace Engineer, a.i. solutions, Inc., Lanham, MD 20706

because of its use of Hill's equations, this method cannot be used on highly non-linear systems. Beard, et al.<sup>2</sup> also considered the problem of formation reconfiguration, but this time the dynamical system was field free space. Another work on formation initialization utilized the non-linear two-body model and primer vector theory to solve the problem impulsively<sup>3</sup>.

This paper considers the development of a tool to optimize the deployment of a formation of spacecraft utilizing relative targeting conditions for the final formation. It consists of a fully non-linear system of relative dynamics in a rotating frame relative to a reference orbit. Indirect methods utilizing calculus of variations are used to construct a minimum-fuel, time-constrained optimization problem for  $n$  spacecraft. The size and shape of the formation are determined by specification of the size of the inter-spacecraft vectors and the angles between them. The velocities of the spacecraft are targeted so as to initialize a formation where the distances between the spacecraft remain constant.

One of the advantages of this method is that using relative targeting conditions creates an increased number of possible solutions by allowing the orientation of the formation to vary. It also allows the formation to be rotating or translating, rather than being forced to remain fixed to a given reference frame. This increases the size of the solution space dramatically. Another advantage of this method is that by using a fully non-linear set of relative accelerations, the reference orbit is not constrained to adhere to any particular dynamical model. This method can be used for all types of Keplerian orbits and all types of LPO's.

The following section details the development of the non-linear relative equations of motion for the system. The equations of motion are derived for two separate relative reference frames: a position referenced frame, and a velocity referenced frame. The Optimal Control Problem section details the derivation of the optimal control problem, using calculus of variations, primer vector theory and the Pontryagin Maxim Principle. This section also sets up the two point boundary value problem, and lists the associated guess and constraint vectors. The Results section shows four different optimal solutions of the formation deployment problem. Three spacecraft are deployed to an equilateral triangle in each of the reference frames, and four spacecraft are deployed to an equilateral tetrahedron in each reference frame as well. Finally, the Conclusions section details the conclusions that have been drawn as a result of this work, as well as the possible ways that this work can be expanded or improved upon in the future.

## RELATIVE EQUATIONS OF MOTION

To directly analyze the relative motions of a system of spacecraft, the relative equations of motion must be derived, and a rotating reference frame must be defined. For this derivation, the base frame is chosen to be an inertial frame centered at the barycenter of the Sun-Earth/Moon system. For simplicity, the Earth and Moon are lumped together as one mass. In this frame, the assumptions of the Circular Restricted Three Body Problem (CRTBP) are made: that the Earth/Moon and Sun orbit their barycenter in circular, coplanar orbits. However, the mass, distance, and time units remain dimensionalized.

Starting from the context of the base inertial frame, there are two spacecraft, SV1 and SV2, whose inertial position and velocity are given by:

$$\mathbf{r}_i = r_i(t) \quad \dot{\mathbf{r}}_i = \mathbf{v}_i(t) \quad i = 1, 2 \quad (1)$$

and the inertial acceleration of the spacecraft is given by:

$$\ddot{\mathbf{r}}_i = -\frac{\mu_s}{r_{is}^3} \mathbf{r}_{is} - \frac{\mu_e}{r_{ie}^3} \mathbf{r}_{ie} + \mathbf{a}_{oth} \quad i = 1, 2 \quad (2)$$

where the final term,  $\mathbf{a}_{oth}$ , can be any number of perturbation forces, e.g. solar radiation pressure, but in this study, the perturbations are assumed to be zero. SV1, which serves as the origin of the relative frame being defined, can be either be a virtual or real spacecraft. If SV1 represents a real spacecraft, Eq. (2) can include the thrust of the spacecraft as well. From the two spacecraft position

vectors, the relative position is defined as

$$\boldsymbol{\delta r} \equiv \mathbf{r}_2 - \mathbf{r}_1. \quad (3)$$

This equation can then be re-written to express  $\mathbf{r}_2$  as a function of  $\boldsymbol{\delta r}$  expressed in a moving frame. This is given as

$$\mathbf{r}_2 = \mathbf{r}_1 + \mathbf{R}\boldsymbol{\delta r}^r \quad (4)$$

where  $\mathbf{R}$  is the rotation from the moving frame to the inertial, and is given by

$$\mathbf{R} = \begin{pmatrix} \hat{\mathbf{i}} \cdot \hat{\mathbf{r}} & \hat{\mathbf{i}} \cdot \hat{\mathbf{s}} & \hat{\mathbf{i}} \cdot \hat{\mathbf{t}} \\ \hat{\mathbf{j}} \cdot \hat{\mathbf{r}} & \hat{\mathbf{j}} \cdot \hat{\mathbf{s}} & \hat{\mathbf{j}} \cdot \hat{\mathbf{t}} \\ \hat{\mathbf{k}} \cdot \hat{\mathbf{r}} & \hat{\mathbf{k}} \cdot \hat{\mathbf{s}} & \hat{\mathbf{k}} \cdot \hat{\mathbf{t}} \end{pmatrix}. \quad (5)$$

In this work, two relative reference frames are considered: a position-referenced frame, and a velocity referenced frame. Eq. (5) above represents the rotation from the position referenced frame to the inertial. The unit vectors that define both relative frames are shown below in Table 1. The method

Table 1: Relative Frame Unit Vectors

Frame	Unit Vectors		
Position Referenced	$\hat{\mathbf{r}} = \frac{\mathbf{r}_1}{r_1}$	$\hat{\mathbf{s}} = \hat{\mathbf{t}} \times \hat{\mathbf{r}}$	$\hat{\mathbf{t}} = \frac{\mathbf{r}_1 \times \mathbf{v}_1}{ \mathbf{r}_1 \times \mathbf{v}_1 }$
Velocity Referenced	$\hat{\mathbf{u}} = \frac{\mathbf{v}_1}{v_1}$	$\hat{\mathbf{v}} = \hat{\mathbf{w}} \times \hat{\mathbf{u}}$	$\hat{\mathbf{w}} = \frac{\mathbf{r}_1 \times \mathbf{v}_1}{ \mathbf{r}_1 \times \mathbf{v}_1 }$

of derivation for the relative equations of motion for each of the frames is the same, only the defined unit vectors and their derivatives change. Therefore, in this derivation, the position referenced frame will be used, and the velocity referenced frame will be a slight adaptation from this example.

The inertial representation of one object's acceleration relative to another (e.g.  $\ddot{\mathbf{r}}_2$ ), is well known<sup>4</sup>, and is given by the relationship

$$\ddot{\mathbf{r}}_2 = \ddot{\mathbf{r}}_1 + \ddot{\boldsymbol{\delta r}} + 2\boldsymbol{\omega}^r \times \boldsymbol{\delta v} + \dot{\boldsymbol{\omega}}^r \times \boldsymbol{\delta r} + \boldsymbol{\omega}^r \times (\boldsymbol{\omega}^r \times \boldsymbol{\delta r}) \quad (6)$$

where  $\boldsymbol{\delta v}$  is the rate of change of the relative position vector, and  $\boldsymbol{\omega}^r$  and  $\dot{\boldsymbol{\omega}}^r$  are the angular rate and acceleration of the rotating frame, respectively. However, the desired quantity here is the relative acceleration, or  $\ddot{\boldsymbol{\delta r}}$ , so Eq. (6) is re-arranged to reflect this. The relative acceleration is then given by

$$\ddot{\boldsymbol{\delta r}} = (\ddot{\mathbf{r}}_2 - \ddot{\mathbf{r}}_1) - 2\boldsymbol{\omega}^r \times \boldsymbol{\delta v} - \dot{\boldsymbol{\omega}}^r \times \boldsymbol{\delta r} - \boldsymbol{\omega}^r \times (\boldsymbol{\omega}^r \times \boldsymbol{\delta r}) \quad (7)$$

where, again  $\ddot{\mathbf{r}}_2$  and  $\ddot{\mathbf{r}}_1$  are expressed in the inertial frame. Therefore to understand the motion of  $\boldsymbol{\delta r}$  in the rotating frame, the inertial accelerations,  $\ddot{\mathbf{r}}_2$  and  $\ddot{\mathbf{r}}_1$ , must be rotated into the moving frame and the components of  $\boldsymbol{\omega}^r$  and  $\dot{\boldsymbol{\omega}}^r$  must be calculated.

For the purposes of this work, it is convenient to express the angular rate and angular acceleration as a function of the components of the rotation matrix. For brevity, the full derivation is not presented here, but it can be found in other works<sup>5</sup>. This relationship is obtained using several factors, including the properties of rotation matrices and the properties of skew-symmetric matrices. From them, it can be shown that

$$\mathbf{R}^T \dot{\mathbf{R}} = \begin{pmatrix} 0 & -\omega_t & \omega_s \\ \omega_t & 0 & -\omega_r \\ -\omega_s & \omega_r & 0 \end{pmatrix} \quad (8)$$

where  $\omega_r$ ,  $\omega_s$ , and  $\omega_t$  are the components of the vector  $\boldsymbol{\omega}^r$ , expressed in the position referenced frame.

After performing the matrix multiplication and relating the non-zero terms, Eq. (8) can be re-written as

$$\boldsymbol{\omega}^r = \begin{pmatrix} \omega_r \\ \omega_s \\ \omega_t \end{pmatrix} = \begin{pmatrix} \hat{\mathbf{t}} \cdot \frac{d\hat{\mathbf{s}}}{dt} \\ \hat{\mathbf{r}} \cdot \frac{d\hat{\mathbf{t}}}{dt} \\ \hat{\mathbf{s}} \cdot \frac{d\hat{\mathbf{r}}}{dt} \end{pmatrix} = - \begin{pmatrix} \hat{\mathbf{s}} \cdot \frac{d\hat{\mathbf{t}}}{dt} \\ \hat{\mathbf{t}} \cdot \frac{d\hat{\mathbf{r}}}{dt} \\ \hat{\mathbf{r}} \cdot \frac{d\hat{\mathbf{s}}}{dt} \end{pmatrix} \quad (9)$$

Now it is possible to describe the rotation of the moving frame in terms of its unit vectors and their derivatives. By taking the derivative of Eq. (9), the angular acceleration of the moving frame can be determined. It has the following form

$$\dot{\boldsymbol{\omega}}^r = \begin{pmatrix} \dot{\omega}_r \\ \dot{\omega}_s \\ \dot{\omega}_t \end{pmatrix} = \begin{pmatrix} \hat{\mathbf{t}} \cdot \frac{d^2\hat{\mathbf{s}}}{dt^2} + \frac{d\hat{\mathbf{t}}}{dt} \cdot \frac{d\hat{\mathbf{s}}}{dt} \\ \hat{\mathbf{r}} \cdot \frac{d^2\hat{\mathbf{t}}}{dt^2} + \frac{d\hat{\mathbf{r}}}{dt} \cdot \frac{d\hat{\mathbf{t}}}{dt} \\ \hat{\mathbf{s}} \cdot \frac{d^2\hat{\mathbf{r}}}{dt^2} + \frac{d\hat{\mathbf{s}}}{dt} \cdot \frac{d\hat{\mathbf{r}}}{dt} \end{pmatrix}. \quad (10)$$

The derivatives shown in Eqs. (9) and (10) must now be calculated. Based on the unit vector definitions shown in Table 1, these have the form

$$\begin{aligned} \frac{d\hat{\mathbf{r}}}{dt} &= \frac{\dot{\mathbf{r}}}{r} - \frac{\mathbf{r}^T \dot{\mathbf{r}}}{r^3} \mathbf{r} \\ \frac{d\hat{\mathbf{s}}}{dt} &= \frac{d}{dt} \hat{\mathbf{t}} \times \hat{\mathbf{r}} + \hat{\mathbf{t}} \times \frac{d}{dt} \hat{\mathbf{r}} \\ \frac{d\hat{\mathbf{t}}}{dt} &= \frac{\dot{\mathbf{h}}}{h} - \frac{\mathbf{h}^T \dot{\mathbf{h}}}{h^3} \mathbf{h} \end{aligned} \quad (11)$$

where  $\mathbf{h} = \mathbf{r} \times \mathbf{v}$  is the specific angular momentum, and its rate of change is given by

$$\dot{\mathbf{h}} = \mathbf{r} \times \ddot{\mathbf{r}}. \quad (12)$$

Furthermore the second derivatives of the unit vectors are found to be

$$\begin{aligned} \frac{d^2\hat{\mathbf{r}}}{dt^2} &= \frac{\ddot{\mathbf{r}}}{r} - 2\frac{\mathbf{r}^T \dot{\mathbf{r}}}{r^3} \dot{\mathbf{r}} + \left[ 3\frac{(\mathbf{r}^T \dot{\mathbf{r}})^2}{r^5} - \frac{\dot{\mathbf{r}}^T \dot{\mathbf{r}} + \mathbf{r}^T \ddot{\mathbf{r}}}{r^3} \right] \mathbf{r} \\ \frac{d^2\hat{\mathbf{s}}}{dt^2} &= \frac{d^2}{dt^2} \hat{\mathbf{t}} \times \hat{\mathbf{r}} + 2\frac{d}{dt} \hat{\mathbf{t}} \times \frac{d}{dt} \hat{\mathbf{r}} + \hat{\mathbf{t}} \times \frac{d^2}{dt^2} \hat{\mathbf{r}} \\ \frac{d^2\hat{\mathbf{t}}}{dt^2} &= \frac{\ddot{\mathbf{h}}}{h} - 2\frac{\mathbf{h}^T \dot{\mathbf{h}}}{h^3} \dot{\mathbf{h}} + \left[ 3\frac{(\mathbf{h}^T \dot{\mathbf{h}})^2}{h^5} - \frac{\dot{\mathbf{h}}^T \dot{\mathbf{h}} + \mathbf{h}^T \ddot{\mathbf{h}}}{h^3} \right] \mathbf{h} \end{aligned} \quad (13)$$

The fact that  $d^2\hat{\mathbf{t}}/dt^2$  contains the second derivative of  $\mathbf{h}$  indicates that the third derivative of  $\mathbf{r}$  must be calculated. By including these derivatives in Eq. (7), all the terms are now known, and the time history of  $\delta\mathbf{r}$  can be computed.

The unit vector derivatives for the velocity referenced frame are similar in form, and are shown below, in Eqs. (14) and (15).

$$\begin{aligned} \frac{d\hat{\mathbf{u}}}{dt} &= \frac{\dot{\mathbf{v}}}{v} - \frac{\mathbf{v}^T \dot{\mathbf{v}}}{v^3} \mathbf{v} \\ \frac{d\hat{\mathbf{v}}}{dt} &= \frac{d}{dt} \hat{\mathbf{w}} \times \hat{\mathbf{u}} + \hat{\mathbf{w}} \times \frac{d}{dt} \hat{\mathbf{u}} \\ \frac{d\hat{\mathbf{w}}}{dt} &= \frac{\dot{\mathbf{h}}}{h} - \frac{\mathbf{h}^T \dot{\mathbf{h}}}{h^3} \mathbf{h} \end{aligned} \quad (14)$$

$$\begin{aligned}
\frac{d^2 \hat{\mathbf{u}}}{dt^2} &= \frac{\ddot{\mathbf{v}}}{v} - 2 \frac{\mathbf{v}^\top \dot{\mathbf{v}}}{v^3} \dot{\mathbf{v}} + \left[ 3 \frac{(\mathbf{v}^\top \dot{\mathbf{v}})^2}{v^5} - \frac{\dot{\mathbf{v}}^\top \dot{\mathbf{v}} + \mathbf{v}^\top \ddot{\mathbf{v}}}{v^3} \right] \mathbf{v} \\
\frac{d^2 \hat{\mathbf{v}}}{dt^2} &= \frac{d^2}{dt^2} \hat{\mathbf{w}} \times \hat{\mathbf{u}} + 2 \frac{d}{dt} \hat{\mathbf{w}} \times \frac{d}{dt} \hat{\mathbf{u}} + \hat{\mathbf{w}} \times \frac{d^2}{dt^2} \hat{\mathbf{u}} \\
\frac{d^2 \hat{\mathbf{w}}}{dt^2} &= \frac{\ddot{\mathbf{h}}}{h} - 2 \frac{\mathbf{h}^\top \dot{\mathbf{h}}}{h^3} \dot{\mathbf{h}} + \left[ 3 \frac{(\mathbf{h}^\top \dot{\mathbf{h}})^2}{h^5} - \frac{\dot{\mathbf{h}}^\top \dot{\mathbf{h}} + \mathbf{h}^\top \ddot{\mathbf{h}}}{h^3} \right] \mathbf{h}
\end{aligned} \tag{15}$$

The combination of the equations in this section provides a dynamical framework within which the motion of  $\delta \mathbf{r}$  can be computed as a first order system of dimension of  $6n + 6$ , with  $n$  being the number of spacecraft, since the location of the origin of the rotating frame,  $\mathbf{r}_1$ , must also be calculated. This system forms the dynamical foundation on which the optimal control problem of the next section is based.

## OPTIMAL CONTROL PROBLEM

In general terms, the optimal control problem considered here is to maximize the final mass of all the spacecraft in the formation. All spacecraft are assumed to be delivered to the reference orbit by the same launch or transfer vehicle. All spacecraft are assumed to leave the launch/transfer vehicle at the same time, and all are assumed to arrive at the final formation at the same time. The thrust history of each spacecraft is assumed to have a thrust-coast-thrust structure. The characteristics of the formation being targeted are arbitrary, and the formation's location and orientation with respect to the reference orbit are free.

The problem is formulated as a fixed initial, free final time problem. However, the natural dynamics of the system create a problem that must be addressed. Due to the instability near LPO's, the natural tendency is for spacecraft to drift away from a halo orbit. For typical station-keeping maneuvers, that means that the longer the wait between maneuvers, the greater the propellant cost. However, with the implementation relative targeting conditions, it is possible reduce the cost by simply increasing the time-of-flight. This is because the relative targeting conditions allow the formation as a whole to be translating relative to the reference orbit. Therefore, when using a thrust-coast-thrust control, increasing the time-of-flight allows the spacecraft to increase the time of coast arc. Each spacecraft briefly thrusts to begin drifting away from the reference orbit, allows this drift to increase the separation between the spacecraft, and then briefly thrusts again, to achieve the desired formation.

Due to this process, the propellant cost then asymptotically approaches a minimum value. This behavior was discovered by optimizing a series of time-fixed solutions for a three spacecraft formation. Figure 1 shows the total propellant cost for the formation as a function of the time-of-flight. This asymptotic approach to the minimum value creates a point of diminishing returns in terms of reducing the propellant cost. Additionally, controllability creates problems for convergence; as the thrust arcs get shorter, it becomes increasingly difficult for the low-thrust CSI engines to achieve the final formation. Due to the problems with convergence and the diminishing returns on the propellant cost, a limit was placed on the maximum time-of-flight.

## Problem Statement and System Equations

The performance index being considered is the same for both reference frames developed, and is shown below. For a given  $(m_0)_i$ , the performance index is

$$\max J = \sum_1^n (m_f)_i \quad i = 1, 2, \dots, n \tag{16}$$

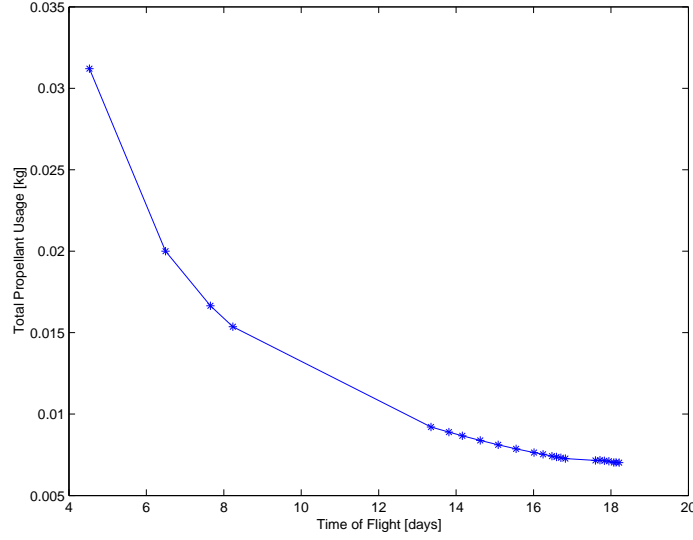


Figure 1: Propellant Consumption vs. Time of Flight

where the state for both frames is

$$\mathbf{X} = \begin{bmatrix} \begin{pmatrix} \delta \mathbf{r}_1 \\ \delta \mathbf{v}_1 \\ m_1 \end{pmatrix} \\ \vdots \\ \begin{pmatrix} \delta \mathbf{r}_n \\ \delta \mathbf{v}_n \\ m_n \end{pmatrix} \end{bmatrix}_{7n \times 1} \quad (17)$$

which is subject to the following differential equations for both the position and velocity referenced frames.

$$\dot{\mathbf{X}} = \begin{bmatrix} \begin{pmatrix} \delta \mathbf{v}_1 \\ (\ddot{\mathbf{r}}_1 - \ddot{\mathbf{r}}_o) - 2\boldsymbol{\omega}^r \times \delta \mathbf{v}_1 - \dot{\boldsymbol{\omega}}^r \times \delta \mathbf{r}_1 - \boldsymbol{\omega}^r \times (\boldsymbol{\omega}^r \times \delta \mathbf{r}_1) + \frac{T_1}{m_1} \hat{\mathbf{p}}_1 \\ -T_1/c_1 \end{pmatrix} \\ \vdots \\ \begin{pmatrix} \delta \mathbf{v}_n \\ (\ddot{\mathbf{r}}_n - \ddot{\mathbf{r}}_o) - 2\boldsymbol{\omega}^r \times \delta \mathbf{v}_n - \dot{\boldsymbol{\omega}}^r \times \delta \mathbf{r}_n - \boldsymbol{\omega}^r \times (\boldsymbol{\omega}^r \times \delta \mathbf{r}_n) + \frac{T_n}{m_n} \hat{\mathbf{p}}_n \\ -T_n/c_n \end{pmatrix} \end{bmatrix}_{7n \times 1} \quad (18)$$

where  $\boldsymbol{\omega}^r$  and  $\dot{\boldsymbol{\omega}}^r$  are determined by the derivatives of the unit vectors of either frame,  $T_i$  is the thrust magnitude,  $\hat{\mathbf{p}}$  is the thrust direction, and  $c_i$  is the exhaust velocity. In both sets of equations of motion, the force model represented by  $\ddot{\mathbf{r}}_i$  and  $\ddot{\mathbf{r}}_o$  is arbitrary, provided it can be integrated. The force model used in this study was given in the previous section by Eq. (2).

The control vector for each spacecraft is the same, and is simply the thrust magnitude and direction.

$$(\mathbf{u}_c)_i = \begin{bmatrix} T_i \\ \hat{\mathbf{p}}_i \end{bmatrix} \quad (19)$$

The controls are constrained by the following equations

$$|\hat{\mathbf{p}}_i| = 1 \quad (20)$$

and

$$0 \leq T_i \leq T_{max}. \quad (21)$$

Next, there is a constraint on the time-of-flight for the deployment, in which a maximum time-of-flight is defined.

$$t_f - t_0 \leq TOF \quad (22)$$

This inequality constraint is converted to an equality constraint using a slack variable, whose optimal value is to be determined.

$$t_f = t_0 + TOF - \gamma^2 \quad (23)$$

And since the initial time is prescribed, the initial state of each spacecraft is prescribed to be the same as the launch/transfer vehicle. This also indicates that there are no conditions that must be enforced at the initial time.

Now the relative constraints that describe the target formation at the final time must be developed. The relative distances between spacecraft and their magnitudes are defined to be

$$\begin{aligned} \boldsymbol{\rho}_1 &= \boldsymbol{\delta r}_{i+1} - \boldsymbol{\delta r}_i \\ \boldsymbol{\rho}_2 &= \boldsymbol{\delta r}_{i-1} - \boldsymbol{\delta r}_i \\ \rho_1 &= |\boldsymbol{\delta r}_{i+1} - \boldsymbol{\delta r}_i| \\ \rho_2 &= |\boldsymbol{\delta r}_{i-1} - \boldsymbol{\delta r}_i| \end{aligned} \quad (24)$$

and the relative velocity between the spacecraft is defined to be

$$\dot{\boldsymbol{\rho}}_1 = \boldsymbol{\delta v}_{i+1} - \boldsymbol{\delta v}_i \quad (25)$$

and the derivative of the magnitude of  $\rho$  is shown below.

$$\dot{\rho}_1 = \frac{\boldsymbol{\rho}_1^\top \dot{\boldsymbol{\rho}}_1}{\rho_1} \quad (26)$$

These quantities are used to define the relative constraints at the final time. These are defined as

$$\boldsymbol{\Psi}_f = \begin{bmatrix} \rho_1 - l_* \\ \dot{\rho}_1 - V_* \\ \frac{\boldsymbol{\rho}_2^\top \boldsymbol{\rho}_1}{|\boldsymbol{\rho}_2| \cdot |\boldsymbol{\rho}_1|} - \cos(\Theta_*) \end{bmatrix}_{3n \times 1} = \mathbf{0} \quad (27)$$

where  $l_*$  is the prescribed relative distance,  $V_*$  is the prescribed rate of change of the magnitude of the inter-spacecraft vectors (nominally set to zero), and  $\Theta_*$  is the prescribed angular separation between the inter-spacecraft vectors. For example, with four spacecraft,  $\Theta_* = 60^\circ$  creates an equilateral tetrahedron. These final conditions will uniquely describe most regular formations of three or more spacecraft.

## Transversality Conditions

In general, the augmented performance index is defined to be

$$\max J' = G + \int_{t_0}^{t_f} [H - \boldsymbol{\lambda}^\top \dot{\mathbf{X}}] dt \quad (28)$$

where  $G$  is defined to be the end point, or Bolza function,  $H$  is defined to be the Hamiltonian, and  $\boldsymbol{\lambda}$  is defined to be the co-states of the problem.  $G$  contains the original performance index

(eg.  $\sum_1^n (m_f)_i$ ), as well as the prescribed final conditions and the inequality constraint on the time-of-flight, which are all added using Lagrange multipliers. In this problem, the Bolza function is

$$G = \sum_1^n (m_f)_i + \boldsymbol{\nu}_f^T \boldsymbol{\Psi}_f + \Theta(t_f - t_0 - TOF + \gamma^2) \quad (29)$$

The Hamiltonian is defined to be

$$H = \boldsymbol{\lambda}^T \mathbf{f} = \sum_1^n (\boldsymbol{\lambda}_r^T \delta \mathbf{v} + \boldsymbol{\lambda}_v^T \delta \mathbf{g} + \frac{T}{m} \boldsymbol{\lambda}_v \hat{\mathbf{p}} - \lambda_m \frac{T}{c})_i \quad (30)$$

where  $\delta \mathbf{g}$  is the relative acceleration in Eq. (18). With the definition of the commonly used Switching Function, the Hamiltonian becomes

$$H = \boldsymbol{\lambda}^T \mathbf{f} = \sum_1^n (\boldsymbol{\lambda}_r^T \delta \mathbf{v} + \boldsymbol{\lambda}_v^T \delta \mathbf{g} + S \cdot T)_i \quad (31)$$

where  $S$ , the Switching Function is

$$S_i = \frac{\lambda_v}{m} - \frac{\lambda_m}{c} \quad (32)$$

The Euler-Lagrange conditions for optimality are derived from the fact that at a minimum, the first differential of the augmented performance index, Eq. (28), is zero as described in Hull<sup>8</sup>. These conditions are shown below

$$\begin{aligned} \dot{\mathbf{X}} &= \mathbf{f} \\ H_{\mathbf{u}_c} &= \mathbf{0} \\ \dot{\boldsymbol{\lambda}} &= -H_{\mathbf{X}}^T \end{aligned} \quad (33)$$

From the Pontryagin Maximum Principle<sup>6</sup>, the spacecraft thrust must be aligned along the primer vector, as defined below.

$$\hat{\mathbf{p}}_i = \begin{pmatrix} \lambda_v \\ \lambda_v \end{pmatrix}_i \quad (34)$$

Then, to maximize the Hamiltonian, the trajectory must have a thrust-coast-thrust structure for Constant Specific Impulse (CSI) engines. Therefore when the Switching Function is positive, the thrust is assigned its maximum value ( $T_{max}$ ), and when the Switching Function is negative, the thrust is assigned its minimum value ( $T_{min} = 0$ ).

The partial derivative of the Hamiltonian with respect to the state yields the equations of motion for the co-states. These are found to be

$$\begin{aligned} (\dot{\boldsymbol{\lambda}}_r)_i &= -(\boldsymbol{\lambda}_v^T \frac{\partial \delta \mathbf{g}}{\partial \delta \mathbf{r}})_i \\ (\dot{\boldsymbol{\lambda}}_v)_i &= -(\boldsymbol{\lambda}_r + \boldsymbol{\lambda}_v^T \frac{\partial \delta \mathbf{g}}{\partial \delta \mathbf{v}})_i \\ (\dot{\lambda}_m)_i &= (\lambda_v \frac{T}{m^2})_i \end{aligned} \quad (35)$$

These equations determine the time histories of all the co-states, and returning to the first differential leads to the natural boundary conditions.

Additionally, if the first differential is to be zero, all the components of the Bolza function (Eq. (29)) must be zero. Therefore, the conditions at the final time must be

$$\begin{aligned} H_f &= G_{t_f} \\ \boldsymbol{\lambda}_f &= G_{\mathbf{X}_f}^T. \end{aligned} \quad (36)$$

When these conditions are in turn applied to the problem under consideration, the following are obtained

$$G_{\mathbf{X}_f}^\top = \begin{bmatrix} (\lambda_{\mathbf{r}f})_i \\ (\lambda_{\mathbf{v}f})_i \\ (\lambda_{mf})_i \end{bmatrix}_{7n \times 1} = \begin{bmatrix} (\frac{\partial \Psi_f}{\partial \mathbf{r}})_i \\ (\frac{\partial \Psi_f}{\partial \mathbf{v}})_i \\ (1)_i \end{bmatrix}_{7n \times 1} \quad (37)$$

$$H_f = -\Theta \quad (38)$$

Eq. (38) indicates that the final value of the Hamiltonian should be equal to  $\Theta$ , the Lagrange multiplier applied to the constraint on the time-of-flight. Also, Eq. (37) shows that the final value of the mass co-state is equal to one.

The inclusion of the inequality constraint, Eq. (23), in the optimization problem leads to two more terms that must be zero in order for the first differential of the performance index to also be zero. These terms that also must be zero are

$$G_\Theta = t_f - t_0 - TOF + \gamma^2 = 0 \quad (39)$$

$$G_\Theta = -2\Theta\gamma = 0. \quad (40)$$

The first equation above will always be zero at the minimum, because at that point, the slack variable,  $\gamma$ , will have its optimal value which will ensure a zero value for the equation. The second equation above must also be zero for an optimal solution. This indicates that either  $\Theta$  or  $\gamma$  must be zero. If  $\Theta$  is zero, this indicates an off-boundary solution, where a natural minimum was found with a time-of-flight less than the maximum specified. If  $\gamma$  is zero, this indicates an on-boundary solution, where the minimum occurs at the maximum time of flight.

## The Boundary Value Problem

The development of the transversality conditions in the previous section leads to the formation of the boundary value problem, which is discussed in this section. The vector of initial unknowns for the boundary value problem is

$$\mathbf{Z} = [ \alpha_n \quad \beta_n \quad \dot{\alpha}_n \quad \dot{\beta}_n \quad (\lambda_v)_n \quad (\dot{\lambda}_v)_n \quad (t_a)_n \quad (t_b)_n \quad \boldsymbol{\nu}_{3n \times 1} \quad \Theta \quad t_f ]_{1 \times (11n+2)}^\top \quad (41)$$

where some of the above quantities were defined in previous section. However, there are several quantities above that have not been defined. These are  $\alpha_n$ ,  $\beta_n$ ,  $\dot{\alpha}_n$ ,  $\dot{\beta}_n$ ,  $(\lambda_v)_n$ ,  $(\dot{\lambda}_v)_n$ ,  $t_a$ , and  $t_b$ . The quantities  $\alpha_n$  and  $\beta_n$  are the spherical angles that describe the thrust vectors of each spacecraft in a body-fixed frame. Their derivatives represent the rates of change for these angles. The quantities  $(\lambda_v)_n$  and  $(\dot{\lambda}_v)_n$  represent the magnitude of the primer vector and its derivative for each spacecraft. These six quantities are used with the Adjoint Control Transformation<sup>9</sup> to form an initial guess for the co-states of each spacecraft. Finally,  $t_a$ , and  $t_b$  represent the beginning and end of the coast arc for each spacecraft. All the spacecraft start and end the deployment with their engines on, but each determines the optimal length of their coast arc. Setting up the boundary value problem in this way assumes a thrust-coast-thrust structure as defined by Lawden<sup>7</sup>.

The optimality of these unknowns are evaluated against the conditions derived in the previous section. The constraint vector is shown below

$$\mathbf{C} = [ (\boldsymbol{\Psi}_f)_{3n \times 1} \quad (S_a)_n \quad (S_b)_n \quad (\lambda_f - G_{\mathbf{X}_f}^\top)_{6n \times 1} \quad H_f + \Theta \quad -2\Theta\gamma ]_{1 \times (11n+2)}^\top = \mathbf{0} \quad (42)$$

where  $\boldsymbol{\Psi}_f$  is the vector of the relative position and velocity constraints imposed on the formation. The quantities  $S_a$  and  $S_b$  are the values of the Switching Function for each spacecraft at the beginning and end of their coast arcs. This indicates the values of the Switching Functions at these times are constrained to be zero. The two vectors shown above in Eqn. (41) and Eqn. (42) form a well-defined two point boundary value problem, and were used to obtain the numerical results shown in the following section.

## RESULTS

Several example solutions are presented in this section. The two-point boundary value problem from the previous section was solved using the NS11AD non-linear equation solver that is provided by the HSL Archive<sup>10</sup>. Deployments of three and four spacecraft were considered. The three spacecraft deployments were to a target formation of an equilateral triangle, and the four spacecraft deployments were to a target formation of an equilateral tetrahedron. Additionally, to be considered in formation, the derivative of the magnitude of the inter-spacecraft vectors must be zero (Eq. (27)). For each formation, the reference orbit was chosen to be a halo orbit about  $L_2$  with a Z-amplitude of  $5 \times 10^5$  kilometers. Figure 2 shows the reference orbit in the CRTBP frame.

For this work, all the member spacecraft in the formation are assumed to be identical in terms of mass and engine performance. The spacecraft have an initial mass of 100 kilograms, and a low-thrust, CSI engine. There are no restrictions placed on the thrust direction. The thrust is allowed to follow the primer vector without any sort of gimbal limits. The engine of each spacecraft is assumed to have a Specific Impulse of 1000 seconds and a Thrust of 0.000025 Newtons. The fixed initial time for these solutions was chosen to be at the positive X-Z plane crossing of the halo orbit. The maximum time-of-flight for these deployments was set to 7 days, and all solutions were driven to the maximum time-of-flight. All spacecraft depart the launch/transfer vehicle at the initial time, and all spacecraft arrive at the final formation at the same time. A thrust-coast-thrust control law is implemented for all solutions.

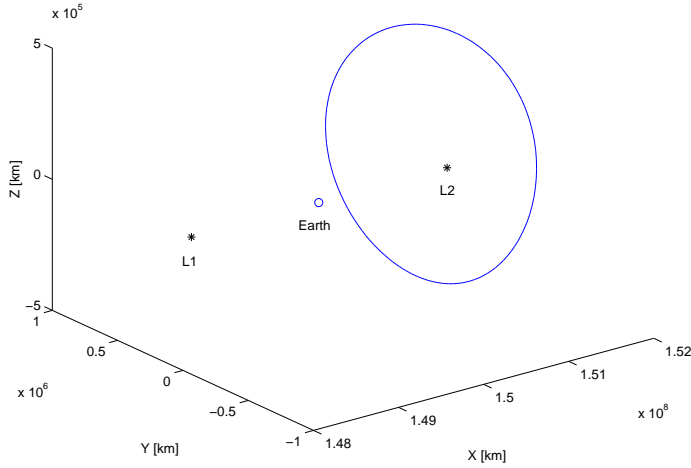


Figure 2: Reference Halo Orbit in CRTBP Frame

### Three Spacecraft Deployments

Figure 3 shows the deployment of three spacecraft to the formation of an equilateral triangle with a side length of 300 km in the position-referenced  $(\hat{r}\hat{s}\hat{t})$  frame. The spacecraft trajectories are shown as the blue dotted lines, with the black arrows indicating the direction of motion. The thrust arcs of each trajectory are shown as red arrows (indicating thrust direction), and the inter-spacecraft vectors of the final formation are shown as the black solid lines. It can be seen from Figure 3 that all the spacecraft travel similar distances away from the launch/transfer vehicle, which is located at the origin. This suggests that the propellant consumption across all three spacecraft is similar, a fact that can also be seen from Table 2, where the actual propellant consumption is given.

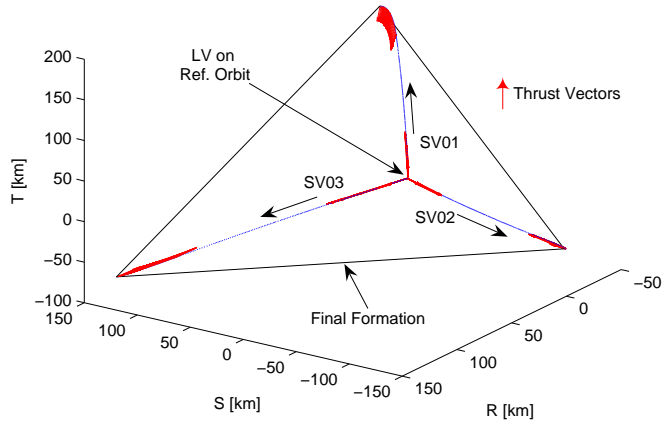


Figure 3: Three Spacecraft Deployment in  $\hat{r}\hat{s}\hat{t}$  Relative Frame

Figure 4 shows the Switching Functions and propellant consumption for all three spacecraft over the course of the deployment. It can be seen that the Switching Functions are of the structure required for optimality, in that they are positive during the thrust arcs, and negative during the coast arc. By comparing the two subplots of the figure, it can be seen that the propellant consumption corresponds to the thrust structure determined by the Switching Functions.

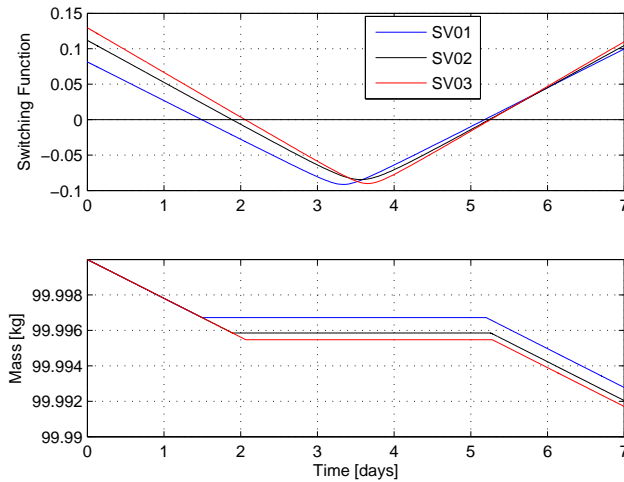


Figure 4: Three Spacecraft Switching Functions & Propellant Consumption ( $\hat{r}\hat{s}\hat{t}$  Case)

Figure 5 shows the problem Hamiltonian for the three spacecraft deployment in the position-referenced frame. It can be seen that the overall magnitude of the Hamiltonian is very small. This is due to two factors, the dynamical system and the relative accelerations used in this work. The Hamiltonian derives a significant portion of its magnitude from the size of the accelerations the spacecraft undergo. Therefore, due to the low acceleration environment in the vicinity of libration points, and the fact that accelerations are calculated relative to the reference orbit, the Hamiltonian is considerably smaller than what is seen in other optimization problems.

Additionally, it can be seen from Figure 5 that the Hamiltonian does indeed vary with time, as was stated previously. However, it should be noted that it does vary continuously over the spacecraft deployment, which indicates that the spacecraft are indeed beginning and ending their coast arcs at the optimal times. If any spacecraft were to start or stop thrusting when the Switching Function is non-zero (see Eq. (31)), there would be a discrete jump in the value of the Hamiltonian.

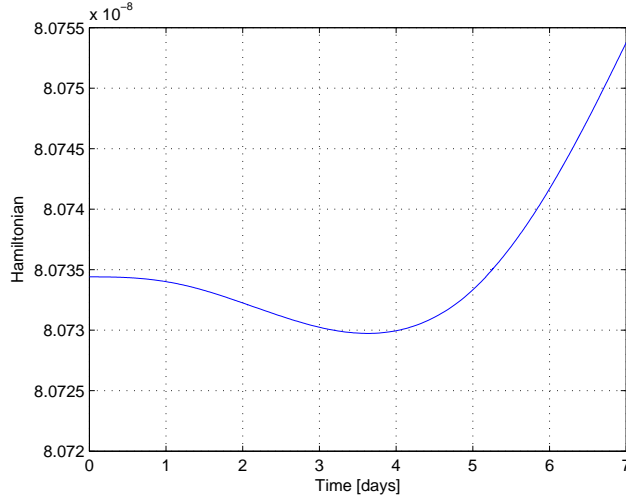


Figure 5: Three Spacecraft Hamiltonian ( $\hat{\mathbf{r}}\hat{\mathbf{s}}\hat{\mathbf{t}}$  Case)

Finally, a note on the distribution of the propellant cost across the formation. From Table 2, it can be seen that the propellant cost is distributed among the three spacecraft in an approximately even fashion. The difference between the maximum and minimum is about 13%. Generally, it was found that for most of the three spacecraft deployments, the propellant consumption varied by approximately 10% to 15%. This is at least partially due to two factors. The first is that it is essentially a planar formation; the next section, with its three dimensional formation, helps to illustrate this by contrast. Second is the tendency of the spacecraft to drift away from the reference halo orbit. These dynamics seem to help prevent any of the spacecraft from remaining in the vicinity of the reference orbit.

Table 2: Propellant Usage: Three Spacecraft  $\hat{\mathbf{r}}\hat{\mathbf{s}}\hat{\mathbf{t}}$  Case

	SV1	SV2	SV3	Total
Prop (kg)	0.00729234	0.00803130	0.00836563	0.02368927

Below, in Figures 6 through 8, a similar three spacecraft deployment is detailed in the velocity referenced ( $\hat{\mathbf{u}}\hat{\mathbf{v}}\hat{\mathbf{w}}$ ) frame. It can be seen that the conditions for optimality were met. While the results are similar, the solutions are different in a couple of ways. First, by comparing Figures 6 and 3, it can be determined that the orientation of the two formations are different. Secondly, comparing Figure 7 to Figure 4, it can be seen that the structure of the Switching Functions for each solution are different. This leads to a difference in the distribution of propellant cost. In this case, the cost varied by less than 12% across all three spacecraft. Additionally, the total cost is about 0.5% higher for the solution presented in the velocity referenced frame.

## Four Spacecraft Deployments

Figure 9 shows the deployment of four spacecraft to an equilateral tetrahedron with a side length of 300 kilometers. The trajectories, thrust arcs and inter-spacecraft vectors are all shown

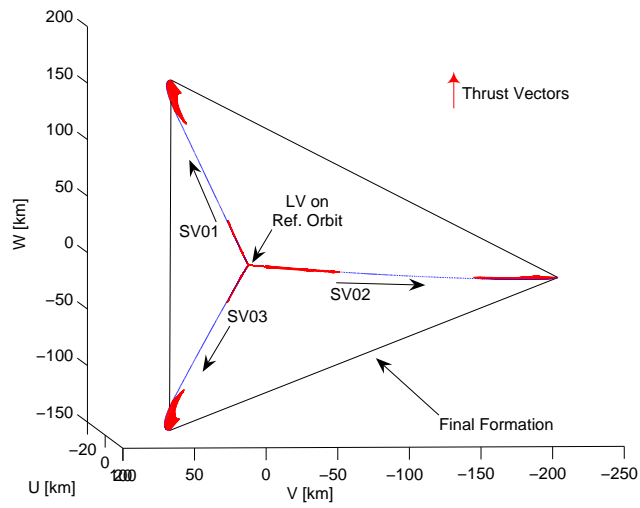


Figure 6: Three Spacecraft Deployment in  $\hat{u}\hat{v}\hat{w}$  Relative Frame

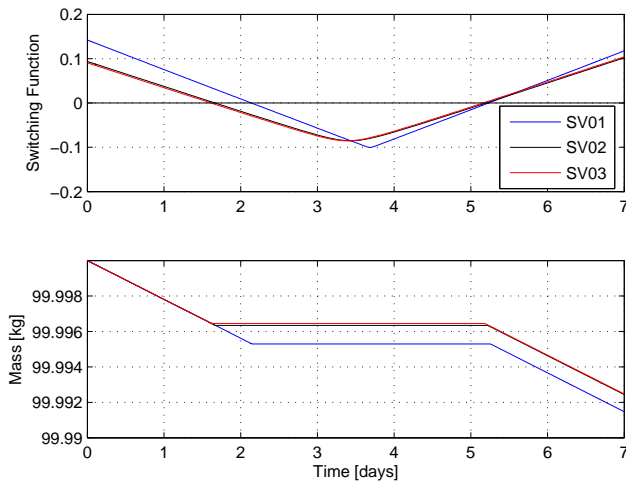


Figure 7: Three Spacecraft Switching Functions ( $\hat{u}\hat{v}\hat{w}$  Case)

Table 3: Propellant Usage: Three Spacecraft  $\hat{u}\hat{v}\hat{w}$  Case

	SV1	SV2	SV3	Total
Prop (kg)	0.00859831	0.00763178	0.00759996	0.02383006

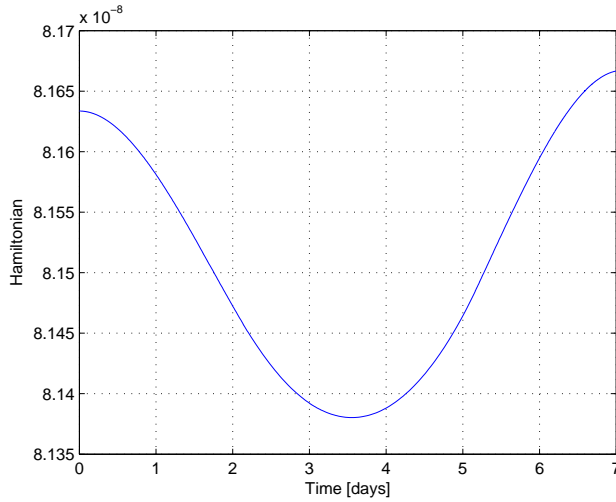


Figure 8: Three Spacecraft Hamiltonian ( $\hat{u}\hat{v}\hat{w}$  Case)

in the same way as before. It can be seen from this figure that one of the spacecraft (in this case it is SV03), travels a considerably shorter distance than the others. This leads to shorter thrust arcs and less propellant consumption, as can be seen in Figure 10. This seems to be due to the fact that the spacecraft are being deployed to a three-dimensional formation in this case. With a planar formation, it is possible for the orientation of the formation to be dictated by the drift of the spacecraft. However with one spacecraft now required to be in a different plane, the thrust requirements for that spacecraft can change considerably.

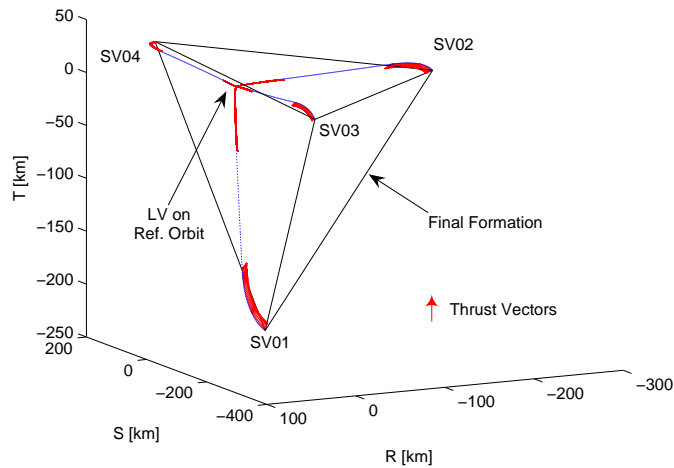


Figure 9: Four Spacecraft Deployment in  $\hat{r}\hat{s}\hat{t}$  Relative Frame

Figure 10 shows the Switching Functions and propellant consumption for all four spacecraft. As with the three spacecraft case, it can be seen that all four spacecraft begin and end their coast arcs according to the Switching function. It can also be seen that SV03 ends its initial thrust arc nearly a full day before the other spacecraft. Because of this, the propellant consumption for the formation, shown in Table 4, is not as evenly distributed for this case. The propellant consumption varies by as

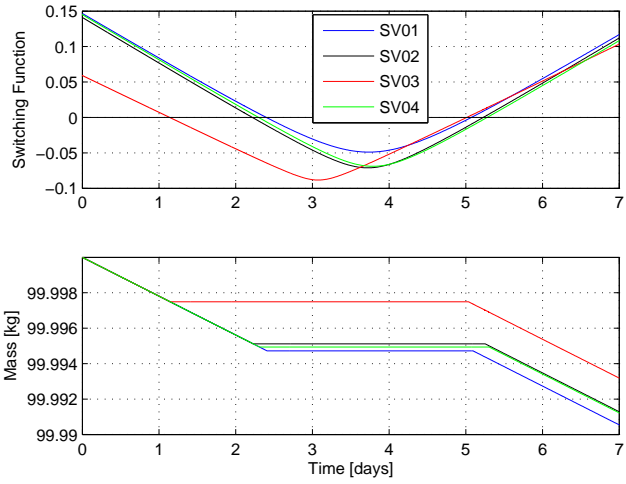


Figure 10: Four Spacecraft Switching Functions ( $\hat{r}\hat{s}\hat{t}$  Case)

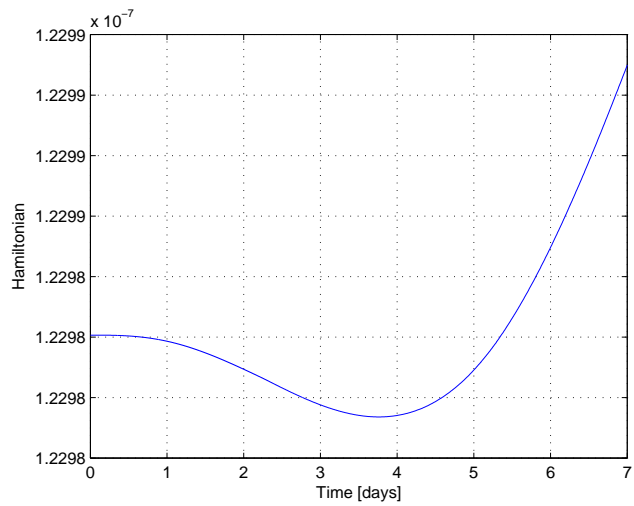


Figure 11: Four Spacecraft Hamiltonian ( $\hat{r}\hat{s}\hat{t}$  Case)

much as 30%, or more than twice what was seen in the three spacecraft deployments. Such an uneven distribution of propellant indicates a need for an inequality constraint to equalize the propellant cost across all the spacecraft. Finally, Figure 11 shows the Hamiltonian for the four spacecraft deployment in the position referenced frame. One item worth noting about the Hamiltonian for this solution is that it is larger than the Hamiltonians for the three spacecraft solution. Since each solution's Hamiltonian is simply a sum of the Hamiltonians for each spacecraft, it gets larger with the addition of more spacecraft.

Table 4: Propellant Usage: Four Spacecraft  $\hat{r}\hat{s}\hat{t}$  Case

	SV1	SV2	SV3	SV4	Total
Prop (kg)	0.00952757	0.00878545	0.00688612	0.00885169	0.03405085

Figures 12 through 14 show the solution for a four spacecraft deployment to an equilateral tetrahedron with a side length of 300 kilometers. This time the solutions were computed in the velocity referenced ( $\hat{u}\hat{v}\hat{w}$ ) frame. This solution is again very similar to the four spacecraft solution presented previously. In this case the distribution of propellant cost varied by as much as 25%, which is a little less than the previous solution, but still larger than the three spacecraft solutions. Looking at the Switching Functions and propellant costs for both four spacecraft solutions, it can be seen that these solutions are very similar in terms of their thrust profile and cost distribution. Additionally, the total propellant cost between the solutions varied by only 1.2%.

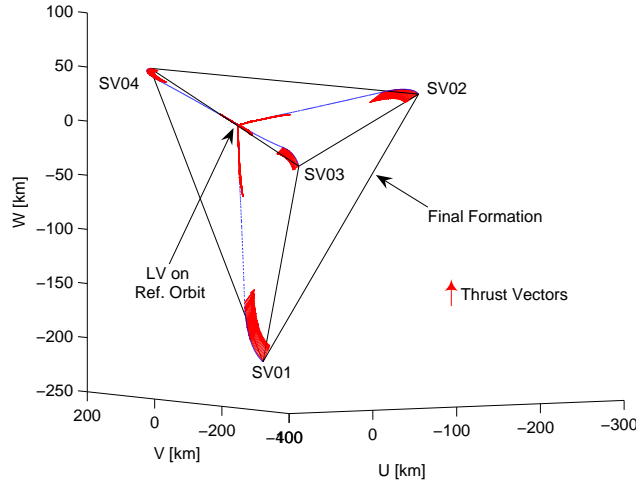


Figure 12: Four Spacecraft Deployment in  $\hat{u}\hat{v}\hat{w}$  Relative Frame

Table 5: Propellant Usage: Four Spacecraft  $\hat{u}\hat{v}\hat{w}$  Case

	SV1	SV2	SV3	SV4	Total
Prop (kg)	0.00929355	0.00849212	0.00703885	0.00880323	0.03362776

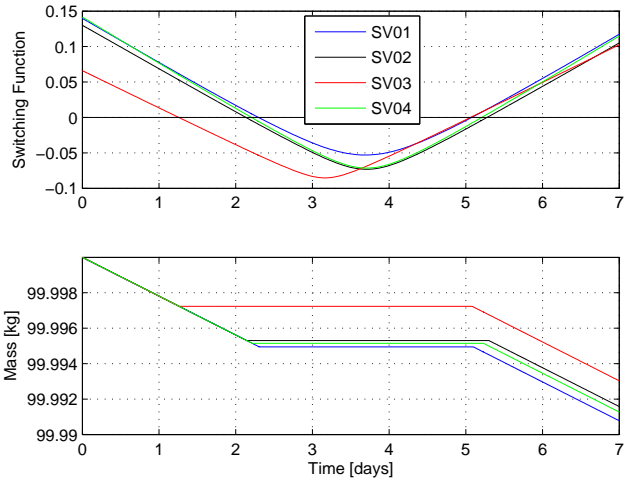


Figure 13: Four Spacecraft Switching Functions ( $\hat{\mathbf{u}}\hat{\mathbf{v}}\hat{\mathbf{w}}$  Case)

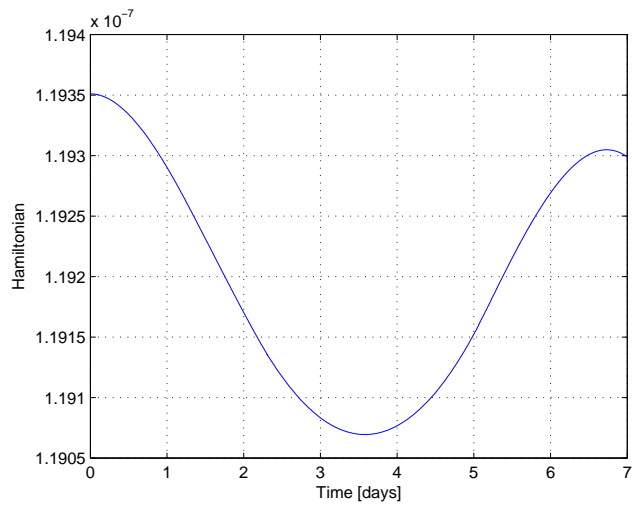


Figure 14: Four Spacecraft Hamiltonian ( $\hat{\mathbf{u}}\hat{\mathbf{v}}\hat{\mathbf{w}}$  Case)

## CONCLUSIONS & FUTURE WORK

### Conclusions

The methodology presented in this work forms a framework that can be used to optimize the deployment of a formation of spacecraft. All aspects of the optimization problem defined within the relative frame. The equations of motion and the spacecraft co-states are all defined relative to the reference orbit. This framework is independent of orbit type, in that it can be applied to various orbit types. No assumptions are made about the dynamical model or size or shape of the reference orbit. In this case, the orbit regime used is the vicinity of the  $L_2$  libration point, and in particular a halo orbit.

Additionally, the final targeting conditions for the formation are relative to the other spacecraft, rather than states in absolute space. This allows the final formation to be either translating or rotating in space. Additionally, this allows for multiple solutions that satisfy the conditions for optimality for any given time-of-flight. These unique consequences of the relative targeting conditions create a very large solution space, allowing for more flexibility regarding the deployment of the formation.

The deployment of three and four spacecraft formations were optimized using this method. Three spacecraft were deployed to an equilateral triangle, and four spacecraft were deployed to an equilateral tetrahedron. Different solutions for each formation were obtained in each relative reference frame. Each solution converged to sub-millimeter levels in position, and micrometers per second in velocity. These solutions were then compared and contrasted in terms of overall propellant cost, as well as the distribution of the cost over the formation.

Both of the three spacecraft solutions shown in the previous section had very similar total propellant costs. The same can be said for the four spacecraft solutions as well. Given that these pairs of solutions varied by about 1% in total cost, it seems that the reference frame and the orientation of the final formation are not significant drivers of the propellant cost. Compare those differences with the data shown in Figure 1, and it seems that the time-of-flight is one of the primary drivers of propellant cost when operating in the vicinity of a halo orbit, and using relative targeting constraints.

Also, the four spacecraft solutions indicated that there is a need to include a constraint to equalize the propellant costs across the formation. A 30% difference in propellant consumption between spacecraft is significant, and if repeated over many maneuvers, could lead to the early loss of one of the spacecraft. This would at the very least diminish the capabilities of the formation, if not render it ineffective.

This methodology was found to be a viable way to optimize the deployment of a formation of spacecraft about a halo orbit. This method has advantages and disadvantages, but was generally found to be a flexible and versatile tool for considering the optimization of formation deployment.

### Future Work

This was a preliminary work with regard to this methodology. One of the primary goals was to simply examine the feasibility of optimizing a formation's deployment using relative constraints. Due to the preliminary nature of this work, there were several simplifying assumptions made. As a result, there are several different ways that this work can be improved or expanded upon. Several avenues of future study are listed below.

- The optimization problem could be generalized to a completely time-free problem, instead of the fixed-initial, free-final time problem discussed here.
- A more realistic deployment scenario could be created, allowing the spacecraft to leave the launch/transfer vehicle individually.
- Additional control laws could be added, such as a continuous thrust law (i.e. no coast arc) for either a CSI or Variable Specific Impulse (VSI) engine.

- The framework of relative accelerations in a relative frame could be generalized with regard to the force model of the reference orbit.
- A more global search of the large solution space could be obtained through the use of a genetic algorithm.
- Additional constraints could be added, such as a constraint to equalize propellant consumption, or a constraint to enforce a minimum range between spacecraft during the deployment.

## References

- [1] Yang, G., Yang, Q., Kapila, V., Palmer, D., and Vaidyanathan, R. "Fuel Optimal Manoeuvres for Multiple Spacecraft Reconfiguration Using Multi-Agent Optimization," *International Journal of Robust and Nonlinear Control*, Vol. 12, n. 2-3, pp. 243-283, February/March 2002.
- [2] Beard, R., and Hadaegh, F., "Fuel Optimized Rotation for Satellite Formations in Free Space," *Proceedings of the American Control Conference*, San Diego, CA, pp. 2975-2979, June 1999.
- [3] Mailhe, L., Schiff, C., and Folta, D., "Initialization of a Formation Using Primer Vector Theory," *International Symposium Formation Flying Missions and Technologies*, Centre National d'Etudes Spatiales Toulouse Space Centre - France, October 29-31, 2002.
- [4] Wiesel, W. E., *Spaceflight Dynamics*, 2nd Edition, Irwin-McGraw-Hill, 1997.
- [5] Ocampo, C., Guinn, J., Breeden, J. "Rendezvous Options and Dynamics for Mars Sample Return Mission", *Advances in the Astronautical Sciences*, v. 109 n. 2, pp. 1661-1680, American Astronautical Society, 2002.
- [6] Pontryagin, L.S., Boltyanski, V.G., Gamkrelidze, R.V., and Mishchenko, E.F., *The Mathematical Theory of Optimal Processes*, Wiley-Interscience Publishers, New York, NY, 1962.
- [7] Lawden, D., *Optimal Trajectories for Space Navigation*, London Butterworths, 1963.
- [8] Hull, D. G., *Optimal Control Theory for Applications*, Springer. New York, 2003.
- [9] Dixon, L.C., and Bartholomew-Biggs, M.C., "Adjoint Control Transformations for Solving Practical Optimal Control Problems", *Optimal Control Applications and Methods*, Vol. 2, 1981, 365-381.
- [10] "NS11AD - ns11.pdf," *HSL Archive*, <http://hsl.rl.ac.uk/archive/hslarchive.html>